Revista Brasileira de Climatologia
Brazilian Journal of Climatology

OPEN ACCESS

DOI: 10.5380/abclima

SEASONAL VARIATION OF CANOPY LAYER HEAT ISLAND AT DISTINCT LOCAL CLIMATE ZONES IN A TROPICAL COASTAL CITY

VARIAÇÃO SAZONAL DA ILHA DE CALOR DA CAMADA DE DOSSEL EM ZONAS CLIMÁTICAS LOCAIS DISTINTAS EM UMA CIDADE LITORAL TROPICAL

VARIACIÓN ESTACIONAL DE LA ISLA DE CALOR DE LA CAPA DE DOSEL EN ZONAS CLIMÁTICAS LOCALES DISTINTAS EN UNA CIUDAD COSTERA TROPICAL

Camila Tavares Pereira
Universidade Federal de São Carlos
tavares.camila88@gmail.com

Vandoir Bourscheidt
Universidade Federal de São Carlos
vandoir@gmail.com

Érico Masiero
Universidade Federal de São Carlos
ericomasiero@yahoo.com.br

Abstract: This work examines the characteristics of the seasonal canopy layer heat island (UHI_{UCL}) in a medium-sized coastal city in the state of São Paulo using the Local Climate Zones approach. The present analysis is based on datalogger campaign conducted from 15th November 2017 to 11th October 2018, complemented by full meteorological data from two stations, one inside the urban area and other in the vicinities (used as the reference station). A careful analysis was conducted to select the more representative days (minimum cloudiness, homogeneous solar radiation, and no/low wind), and the resulting dataset was organized in two seasons: summer and winter. Based on the UHI intensity analysis, the results indicate that, during the night period, the temperature anomaly (UHI_{UCL}= LCZx - LCZy) is higher in the compact high-rise buildings and during the winter. During daytime, the

maximum was found in compact low-rise building and for summer period, although strong variations where observed. Those variations seem to be related with the patterns of solar exposure, shading, and vegetation of each area, but may also be associated with the differences observed between the urban and reference station. This suggests that UHI intensity analysis during daytime strongly depends on complete meteorological information.
Keywords: Canopy layer heat island. Local Climate Zones. Meteorological data.

Resumo: Este trabalho avalia as características sazonais da Ilha de Calor na camada de dossel (UHI_{UCL}) em uma cidade costeira de médio porte do estado de São Paulo usando a abordagem de Zonas Climáticas Locais (*LCZ*). O presente estudo baseia-se em medições microclimáticas por meio de *dataloggers* realizadas entre 15 de novembro de 2017 a 11 de outubro de 2018, e complementada por dados meteorológicos de duas estações, uma dentro da zona urbana e outra nas proximidades (utilizada como referência). Uma análise cuidadosa foi conduzida para selecionar os dias mais representativos (céu claro com poucas nuvens, radiação solar homogênea e sem vento ou vento fraco), e o conjunto de dados resultante foi organizado em duas estações: verão e inverno. Com base na análise de intensidade da *UHI*, os resultados indicam que, durante o período noturno, a anomalia de temperatura (UHI_{UCL} = LCZx - LCZy) é maior durante o inverno nos edifícios altos e compactos. No verão, durante o período da tarde, o maior valor foi encontrado nos edifícios baixos e compactos, embora com variações da intensidade da *UHI*. Essas alterações parecem estar relacionadas aos padrões de exposição solar, sombreamento e vegetação de cada área, mas também podem estar associadas às diferenças observadas entre a estação urbana e a de referência. Isso sugere que a análise de intensidade de UHI durante o dia depende fortemente de informações meteorológicas completas.
Palavras-chave: Ilha de calor da camada de dossel. Zonas Climáticas Locais. Dados meteorológicos.

Resumen: Este trabajo examina las características de la isla de calor de la capa de dosel (UHI_{UCL}) en una ciudad costera de tamaño mediano en el estado de São Paulo utilizando el enfoque de Zonas Climáticas Locales. El presente análisis se basa en la campaña de *datalogger* realizada entre el 15 de noviembre de 2017 y el 11 de octubre de 2018, complementada con datos meteorológicos de dos estaciones, una dentro del área urbana y otra en las inmediaciones (utilizada como estación de referencia). Se realizó un análisis cuidadoso para seleccionar los días más representativos (nubosidad mínima, radiación solar homogénea y sin viento / viento suave), y el conjunto de datos resultante se organizó en dos estaciones: verano e invierno. Basado en el análisis de intensidad de UHI, los resultados indican que, durante el período nocturno, la anomalía de temperatura (UHI_{UCL} *= LCZx - LCZy*) es mayor en los edificios compactos de gran altura y durante el invierno. Durante el día, el máximo se encontró en edificios compactos de bajo altura y para el período estival, aunque se observaron fuertes variaciones. Esas variaciones parecen estar relacionadas con los patrones de exposición solar, sombreado y vegetación de cada área, pero también pueden estar asociadas con las diferencias observadas entre la estación urbana y de referencia. Esto sugiere que el análisis de intensidad de UHI durante el día depende en gran medida de la información meteorológica completa.
Palabras clave: Isla de calor de la capa del dosel. Zonas climáticas locales. Datos meteorológicos.

Submetido em: 17/08/2020
Aceito para publicação em: 08/09/2021
Publicado em: 22/09/2021

INTRODUCTION

The urban climate is the product of the alterations that human activities cause in the natural environment. Cities contribute to changes in climate and atmospheric composition on different scales: local, regional, and even globally (OKE *et al*., 2017). Cities are more vulnerable to the effects of these alterations due to the high concentration of people, settlements, and material goods (GEORGESON *et al*., 2016). Therefore, it is in these regions, with a large concentration of people, that the original landscape is transformed most intensely, changing the local climate. In the last decades, by recognizing the harmful effects of urbanization on human health and thermal comfort, numerous surveys have been done in tropical and subtropical cities, mainly regarding the Urban Heat Island (UHI). The importance of UHI in summer and hot climates lays especially on the thermal discomfort (and heat-related health issues) and air quality (SAILOR & DIETSCH, 2007).

There has been a growing interest in the UHI, especially in the Asia-Pacific regions, in cities like Colombo (EMMANUEL, 2003; 2005a,b; EMMANUEL & JOHANSSON, 2006), Kuala Lumpur (TSO, 1996; MORRIS et al., 2015), Singapore (TSO, 1996; NICOL, 1996; WONG *et al*., 2005; CHOW & ROTH, 2006; ROTH & CHOW, 2012), and Hong Kong (GIRIDHARN *et al*., 2004, 2005; NICOL & WONG, 2005; TAN *et al*., 2016). On the other hand, there is a lack of studies on this matter in South America, which is suffering with a disproportionate actual (and projected) urban growth. Few studies were conducted in Argentina (BEJARAN & CAMMILONI, 2003; CAMILLONI & BARRUCAND, 2012), and more recently in Western Pacific cities like Andacollo (CRAWFORD *et al*., 2018), Antofagasta, Lima, Guayaquil, and Valparaiso (PALME *et al*., 2016).

In Brazil, the urban climate trajectory began with the study conducted by Monteiro (1976) related to the conception of Urban Climate System. Since that, the surveys have been evolving and expanding to other interconnected areas, such as UHI, thermal comfort, micro-urban climate, and energy management. Some examples are the works of Lombardo (1984), Assis & Frota (1999), Amorim (2002), Ribeiro (2005), Souza (2007) and Duarte (2010, 2016). More detailed analyzes are, therefore, particularly important in assessing a city's efforts to promote UHI mitigation strategies, and thus the ability of policymakers and citizens to compare different options and predict possible effects (WANG; BERARDI; AKBARI, 2015).

In this context, different activities have been promoting changes in the urban environment and in the microclimate of Santos, a coastal city on the southeast of Brazil. The summer tourism, the petrochemical complex, the regional construction activity, the exploration of oil and gas from Santos Basin, as well as the infrastructure linked to the Port of Santos are some examples of such activities (KAWASHIMA *et al*., 2015). And the different urban patterns imposed by those activities imply in different effects on the UHI, which are usually evaluated through the so-called Local Climate Zones (LCZs) (STEWART & OKE, 2012). LCZ framework has been applied in tropical countries by various researchers, such as Kochi (THOMAS *et al*., 2014), Delhi (SHARMA *et al*., 2016) and Nagpur (KOTHARKAR & BAGADE, 2018) in India, Colombo (PERERA & EMMANUEL, 2016) in Sri Lanka, Hong Kong (SIU & KART, 2013) and Nanjing (YANG *et al*., 2018) in China, and Sao Paulo (FERREIRA & DUARTE, 2019) in Brazil. Therefore, the main goal of the study is to assess the (seasonal) thermal behavior of each LCZs in Santos and the factors that most influence it, focusing not only on heat island magnitudes but also on temperature daily variations between the sites, as well as on the shadow pattern. The climatic effects of the interaction between the main airflow patterns, urban characteristics, and location of different land use categories in Santos are discussed.

STUDY AREA AND METHODS

Study area

Santos, located on the Southern Brazilian Coast, is considered one of the most important municipalities in the State of Sao Paulo. Since its inception, the city has been linked to port activities. Some events related to coffee exportation and railway construction contributed to the incipient urban design of Santos during the 19th century. In the early years of the 20th century, canals were built by Saturnino Brito (sanitary engineer) across the west side to improve sanitation. In the middle of the century, two dichotomous factors drove Santos's urban sprawl. The first, related to the construction of the Anchieta highway and summer tourism, provided the process of verticalization of the waterfront. The second, linked to port labor, boosted the disorderly occupation of the northwest area. These factors have so far contributed to the development of three main areas in Santos's city: (i) the southeastern region, located near the beach, where most investment and economic dynamism are concentrated; (ii) the northern area, which coincides with the old historical nucleus; and (iii)

the northwest region, which concentrates a large number of informal settlements with mostly low-income residents (BLOCH; PAPACHRISTODOULOU; MONROY, 2012).

According to Köppen's climate classification, Santos is within the Af class, characterized by a tropical rainy climate. Based on Miller *et al*. 2012, "the median annual temperature in Santos is around 21.9°C, with a difference of 5°C between summer and winter seasons. On average, Santos receives about 2500 mm of total annual precipitation concentrated from October to April (75%) and an average monthly total of 317 mm". Besides, the proximity of the Atlantic Ocean influences on atmospheric circulation patterns, which play an essential role in climate elements such as temperature, humidity, precipitation, and wind direction. Regarding the ventilation pattern, the alternation of the sea and land breeze establishes a permanent thermal exchange. The sea breeze blowing toward the mainland begins in the late morning and remains acting until the middle of the night when the land breeze starts to dominate until the early morning.

Local Climate Zones

This system was adopted in this study, with the sites characterized accordingly. The aim of the LCZ concept is to enhance the understanding and interpretation of air temperature differences within the urban context and to allow the communication and comparison of results among cities (FENNER *et al*., 2014). The landscape is represented by 17 LCZs, from which 15 are defined by surface structure and cover; and 2 by construction materials and anthropogenic heat emissions. The standard set is divided into "built types" 1–10, and "land cover types". Thus, this new classification leads to a more significant interpretation of UHI intensity through the temperature differences between LCZs and the reference station ($\Delta T = LCZ_{X-Y}$) (STEWART & OKE, 2012). LCZ scheme was proposed to better account for the role that urban morphology plays in the UHI phenomenon and to provide a rich source of information about urban areas that is consistent and comparable among different cities (BECHTEL *et al*., 2019). Our purpose here is not to evaluate the LCZ scheme but to use it to classify the observation sites and to understand the variations among them. The LCZ map was produced in agreement with WUDAPT methodology workflow (BECHTEL *et al*., 2015). It is based on three daytime LANDSAT 8 scenes (July 26th and November 15th, 2017, and August 30st, 2018), on training areas selected in Google Earth, and on the algorithm for Local Climate Zone

classification within the System for Automated Geoscientific Analyses (SAGA) version 6.4. The classification algorithm is the so-called Random Forest classifier, which consists of integrated decision trees that classify each image pixel into one LCZ type. The LCZ map[1] spatial resolution is 100m (Fig. 1)

Figure 1 - Santos - Local Climate Zone Classification. Circles, with radius of 500m, represents LCZs and three official stations used in this study: CETESB, METAR and INMET.

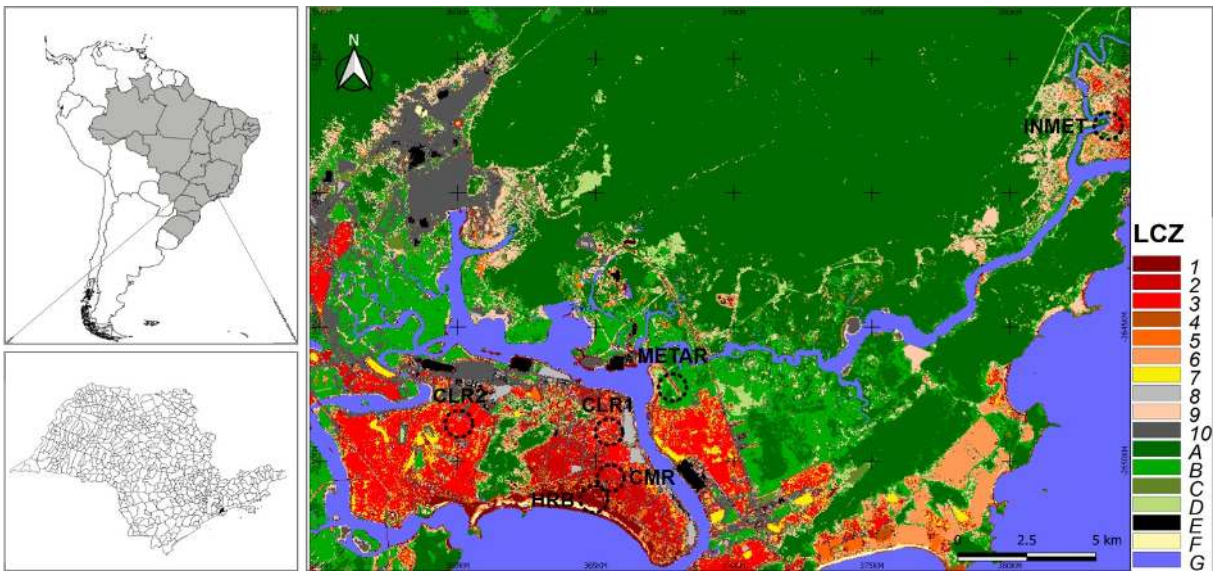

Source: Elaborated by the authors (2020)

Based on the LCZ classification, our sites include compact high-rise, mid-rise and low-rise buildings. Compact high-rise building (HRB) is classified as LCZ1. Compact Mid-rise (CMR) and CETESB as LCZ2 and compact low-rise 1 and 2 as LCZ3 (Fig. 1). The reference station (INMET) was classified as sparsely built (LCZ9). The accuracy of the map was produced by Benjamin Bechtel, which showed Overall Accuracy (OA) of 0.78 and the Kappa coefficient was 0.75 (Fig. 2, left). The Weighted Accuracy (WA) (Fig. 2, right) illustrates a metric that accounts for similarity and dissimilarity between LCZs. For more information see Bechtel *et al*. 2019.

[1] See Bechtel et al., 2019 to assess more information about LCZ workflow and WUDAPT.

Figure 2 - Bootstrapping results for Santos (left); Similarity of LCZ types applied to a weighted accuracy measure (right).

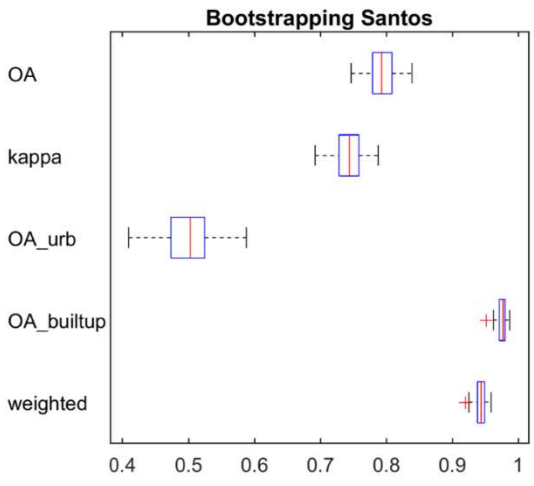

LCZ	1	2	3	4	5	6	7	8	9	10	A	B	C	D	E	F	G
1	1.00	0.92	0.83	0.67	0.58	0.50	0.58	0.75	0.42	0.75	0.33	0.25	0.08	0.00	0.25	0.00	0.00
2	0.92	1.00	0.92	0.58	0.67	0.58	0.67	0.83	0.42	0.83	0.42	0.33	0.25	0.08	0.33	0.08	0.08
3	0.83	0.92	1.00	0.50	0.58	0.67	0.75	0.92	0.58	0.92	0.50	0.42	0.33	0.17	0.42	0.17	0.17
4	0.67	0.58	0.50	1.00	0.92	0.83	0.75	0.50	0.75	0.58	0.50	0.58	0.50	0.33	0.08	0.33	0.33
5	0.58	0.67	0.58	0.92	1.00	0.92	0.83	0.67	0.83	0.67	0.58	0.67	0.50	0.42	0.17	0.42	0.42
6	0.50	0.58	0.67	0.83	0.92	1.00	0.92	0.75	0.92	0.75	0.67	0.75	0.67	0.58	0.25	0.50	0.50
7	0.58	0.67	0.75	0.75	0.83	0.92	1.00	0.67	0.83	0.67	0.75	0.67	0.58	0.42	0.17	0.42	0.42
8	0.75	0.83	0.92	0.50	0.67	0.75	0.67	1.00	0.75	0.92	0.42	0.50	0.42	0.25	0.50	0.33	0.33
9	0.42	0.42	0.58	0.75	0.83	0.92	0.83	0.75	1.00	0.67	0.58	0.67	0.75	0.58	0.33	0.58	0.58
10	0.75	0.83	0.92	0.58	0.67	0.75	0.67	0.92	0.67	1.00	0.42	0.50	0.42	0.25	0.50	0.33	0.33
A	0.33	0.42	0.50	0.50	0.58	0.67	0.75	0.42	0.58	0.42	1.00	0.92	0.83	0.67	0.42	0.67	0.67
B	0.25	0.33	0.42	0.58	0.67	0.75	0.67	0.50	0.67	0.50	0.92	1.00	0.92	0.75	0.50	0.75	0.75
C	0.08	0.25	0.33	0.50	0.50	0.67	0.58	0.42	0.75	0.42	0.83	0.92	1.00	0.83	0.58	0.83	0.83
D	0.00	0.08	0.17	0.33	0.42	0.58	0.42	0.25	0.58	0.25	0.67	0.75	0.83	1.00	0.75	0.92	0.92
E	0.25	0.33	0.42	0.08	0.17	0.25	0.17	0.50	0.33	0.50	0.42	0.50	0.58	0.75	1.00	0.75	0.75
F	0.00	0.08	0.17	0.33	0.42	0.50	0.42	0.33	0.58	0.33	0.67	0.75	0.83	0.92	0.75	1.00	0.92
G	0.00	0.08	0.17	0.33	0.42	0.50	0.42	0.33	0.58	0.33	0.67	0.75	0.83	0.92	0.75	0.92	1.00

Source: Elaborated by the authors (2020)

The OA_urb (Fig. 2, left) is the OA of urban-only reference polygons and thus indicates the quality for the urban classes. The OA_builtup is the overall accuracy of built vs. natural types only, ignoring their internal differentiation. WA is based on the climatic impact discussed in Stewart, Oke, and Krayenhoff (2014) and consists of up to twelve points for the properties openness, height, cover, and thermal inertia, penalizing confusion between dissimilar types more than between similar classes (STEWART, 2016 apud BECHTEL *et al*., 2017). For instance, LCZ 1 is most alike the other two compact urban types (LCZs 2 and 3) and hereafter these pairs have higher weights than classes which are quite different, such as LCZ 1 and the natural types, as LCZ B. The weights are applied to the confusion matrix so that WA measures the accuracy of the LCZ map in terms of the expected thermal impact, rather than the percentage of predicted LCZ values that exactly match those in the reference areas (BECHTEL *et al*., 2017).

Observation sites and daily shadow pattern

The analysis of Santos's microclimate was designed based on the LCZ classification (STEWART & OKE, 2012). Two weather stations and four data loggers[2] represent the variations of different built environments considering their forms, functions, historical processes, and valuation of space. In this way, National Meteorological Institute of Brazil (INMET) and

[2] All data loggers were protected by the Solar Radiation Shield RSI. The solar radiation shield is recommended for temperature and relative humidity measurement accuracy in locations exposed to direct or reflected solar radiation.

Environmental Company of the State of São Paulo (CETESB) were chosen as official stations (Fig. 3). The first one, located in a relatively less occupied area beside a river, situated in Bertioga town (23 km from Santos), was considered as a reference station. The second, located in the middle of the city, was used to validate the data logger measurements. Four data loggers (HOBO Pro v2) distributed across the city were used to capture the response of air temperature and relative humidity for the different LCZ types. For temperature, the accuracy is 0.2°C for the range between 0° to 50°C with 0.02°C of resolution, and for relative humidity the resolution is 0.03% with an accuracy of +/- 2.5% between 10% and 90% RH (typical), to a maximum of +/- 3.5% out of this range. Other two stations were used only to obtain data from cloud cover and precipitation, i.e., METeorological Aerodrome Report (METAR) and National Center for Monitoring and Early Warning of Natural Disasters (CEMADEN), respectively.

Figure 3 - Official stations: CETESB (left) and INMET (right).



Source: Elaborated by the authors (2020)

Three data loggers are positioned in the central-south area, and another in the northwest of Santos urban area. CETESB was selected for validating the measured campaign. The first, compact high-rise building (HRB), located at the seafront, has the prevalence of high-rise commercial and residential buildings, characterized by flats ranging from 50 to 120 m. This area is densely built up on impermeable soils. In relation to green areas, planted trees and patches grass are observed in the horizontal beachfront park, in the drainage canal, and in the walkways. Moreover, it has a large flux of people and vehicles over the entire year, with a significant increase in summer holidays. The second, compact mid-rise building (CMR), located

in a central-south area, is dominated by mid-rise commercial and residential buildings consisting of 3 – 9 floors. Other kinds of urban use are featured in this area, like low-rise residential buildings, warehouses, office blocks and open parking. Like the CMR's urban function, compact low-rise building 1 (CLR1), situated in a central-north portion of Santos, has some particularities that distinguish it from the former, like its position close to the harbor and the presence of smaller buildings. With respect to the green areas, CLR1 has less planted trees, but a considerable number of grass patches. Finally, compact low-rise 2 (CLR2), situated in the northwest side, is dominated by compact low-rise buildings (z = 10 - 14 m) and local markets. A relevant feature of this area is the occupation (starting in the 1950s) without a clear legal urban growth and sprawl regulation, resulting not only in tortuous but also narrow streets. Different from the others, the CLR2 has small quantities of urban parks characterized by both scarce trees and grass patches. Details about the sky view factor (SVF) for all LCZs are shown in Figure 4. The SVF was determined from the images generated by a fisheye lens, attached to a camera, and positioned 1,5m above the ground, aligned vertically upwards. The images were further processed in the Rayman 1.2 computer program developed by Matzarakis (2009), based on recommendations of Matzarakis *et al*. (2010). Morphological characteristics of all sites are summarized in Table 1.

Figure 4 - Sky view factor and general panorama for each LCZ: HRB (top left), CMR and CETESB (bottom left), CLR1 (top right) and CLR2 (bottom right). The red point shows data logger position and localization of the official station (CETESB).

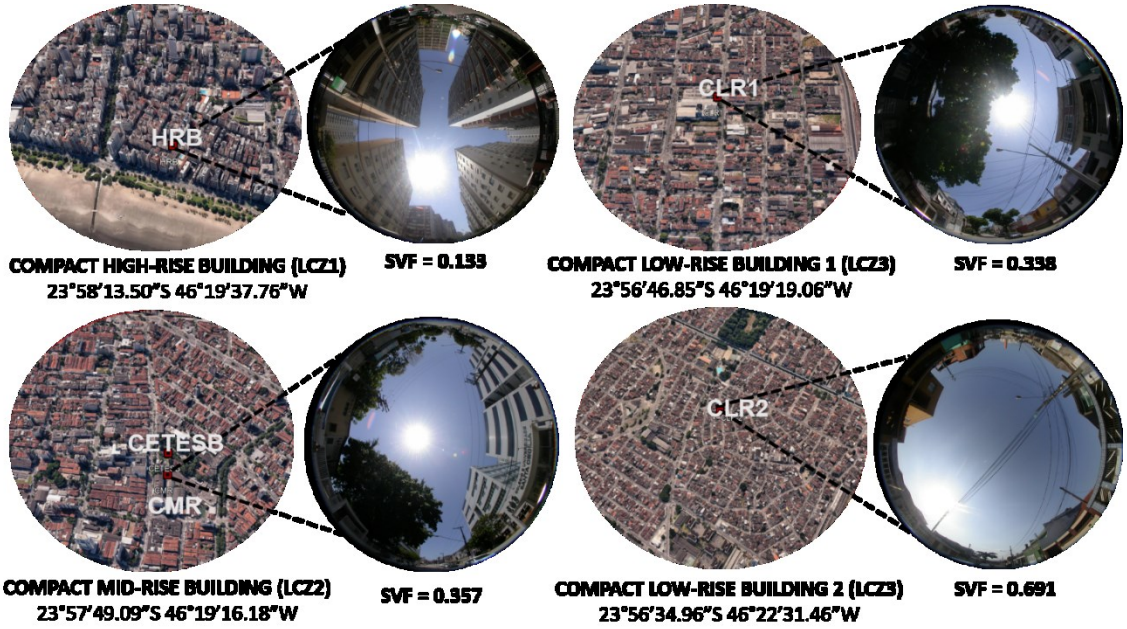

Source: Elaborated by the authors (2020).

Table 1 - Description of morphological features of each official station used and LCZ analyzed in this study.

Site	Sensor Height (m)	Measured data	General urban features of site (within 500m radius)	General vegetation features of site (within 500m radius)	NDVI[3] (within 500m radius)	Coastline distance (km)
CETESB (official station)	3	Temp RH	Mid-rise commercial and residential buildings; shopping malls, universities, office blocks, schools.	Tress planted at irregular intervals on the sidewalks, small gardens spaces in front of houses and commercial buildings. Mature trees planted at regular intervals throughout the drainage canal.	0.27	1,24 (1,76 km from the drainage canal)
METAR (official station)	3	Cloud height Cloud cover	Located in the air base of Santos, it has a warehouse and a runway.	Mixture of bare, soil exposed, grass patches and Atlantic forest patches.	0.78	8,02 (0,7 km from river)
INMET (official station)	3	Temp Rainfall	Mixture of open low-rise residential buildings and warehouses.	Large amount of tress in the garden spaces of houses. Several grass patches and concentrated portions in the north, south and west of Atlantic Forest from site.	0.48	1,13 (0,1 km from the drainage canal)
HRB (DL[4])	4,5	Temp RH	Front of the beachfront has a mixture of both compact high-rise commercial buildings and residential flats, open car parks.	Mixture of open grass and irregular tress planted in the beachfront. Mature trees planted at regular intervals throughout drainage canal. Large amount of tress in sidewalks and in garden spaces of buildings.	0.23	0,16
CMR (DL)	2,5	Temp RH	Mid-rise commercial and residential buildings; shopping malls, universities, office blocks, schools, and municipal offices.	Tress planted at irregular intervals in sidewalks, small gardens spaces in front of houses and commercial buildings. Mature trees planted at regular intervals throughout the drainage canal.	0.27	1,12 (1,96 km from the drainage canal)
CLR1 (DL)	2,5	Temp RH	Mid-rise commercial and residential buildings; shopping malls, universities, office blocks, schools, warehouse, and parking lots.	Numerous small grass patches; Isolated trees in the sidewalks and gardens of houses and commercial buildings. Irregular and sparse trees throughout the drainage canal.	0.26	3,0 (1,2 km from the drainage canal)
CLR2 (DL)	2,5	Temp RH	Low-rise residential with a mixture of small business and plazas.	Numerous small grass patches; sparse trees at the sidewalks and municipal buildings. Plazas with irregular number of planted trees.	0.24	2,8 (1,58 km from the drainage canal)

Source: Elaborated by the authors (2020)

[3] Normalized Difference Vegetation Index (NDVI) calculated by using LANDSAT 8 (17th December 2017).
[4] DL: data loggers

To evaluate the impact of the shade on the temperature variations, we used the Shadow generator plugin in QGIS, which creates pixel wise shadow estimates based on both ground and building/vegetation digital surface models (DSM). The methodology is based on the work of Ratti and Richens (1990) and is further developed and described in Lindberg and Grimmond (2011). In this experiment, daily shadow pattern was determined for all LCZs (CETESB and CMR are the same due to proximity) using integrated building+vegetation DSM. To create the shadow pattern during 08:00 – 17:00, 23rd January was used to represent the summer period and 30th August 2018 was used for winter. Table 2 exhibited the amount of shadow extracted for each LCZ and CETESB for both seasons.

Table 2 - Amount of shadow (in percentage) extracted for each LCZ and CETESB files (hourly) for each season studied.

SEASONS and LCZ(s)	HOURS									
	8	**9**	**10**	**11**	**12**	**13**	**14**	**15**	**16**	**17**
SUMMER										
HRB	46	45	38	30	19	9	21	32	44	47
CTB	43	31	22	15	8	3	11	17	26	36
CLR1	30	20	13	9	5	2	6	10	17	26
CLR2	33	23	15	10	4	1	6	12	18	27
WINTER										
HRB	30	38	46	44	37	41	46	47	49	42
CTB	42	42	32	24	22	22	23	27	36	49
CLR1	49	38	29	23	18	18	21	26	34	46
CLR2	45	30	21	15	13	13	14	18	26	39

Source: Elaborated by the authors (2020)

Seasonal variation of the canopy layer heat island (UHI_{UCL})

The present analysis is based on data logger campaign conducted from 15th November 2017 to 11th October 2018. The resulting dataset has passed through different filtering levels to select the days where all the controls that regulate the canopy-level UHI were ideal, i.e., calm, clear days when the radiation cooling is strong and turbulent mixing is weak (Oke *et al*., 2017). In summary, data was organized in two seasons: summer, from 1st December 2017 to 31st January 2018; and winter, from 1st August to 30st September. The main goal of the

present research is to examine the diurnal thermal behavior of the UHI_{UCL} based on seasons to illustrate changes in development and magnitude. The UHI magnitude for each LCZ was defined as the difference between the maximum LCZ temperature and a temperature of the reference station (INMET – LCZ_9) over a specified period, i.e., $UHI_{UCL,\ max} = LCZ_X - LCZ_9$.

RESULTS

Seasonal variation of the UHI_{UCL}

During the period considered in the analysis, weather conditions varied significantly, with a considerable number of days with rainfall, especially during the summer. As expected, the cloud cover was extensive during the whole considered period and only a few clear days could be selected according to standard definitions (less than 3 octas of cloud cover, see e.g., JONSSON, 2005). For this study, 'clear' days have ≤3 octas, 'partly cloudy' present 5 to 7 octas and 'overcast' > 7 octas. To evaluate both scales for all LCZs and CETESB, only clear days with light wind (<2,5 m/s) and without precipitation were chosen. Therefore, for summer, only 2 days in December and 7 days in January matched this ideal meteorological condition. During winter, only 2 days in August and 3 days in September could be used. Nevertheless, for this selection, based on radiation data from CETESB and INMET, it was possible to observe the influence of cloud cover variation on air temperature between them.

Therefore, to avoid erroneous discussions, we chose the days when the daytime radiation exposure at both official stations was more homogeneous. Figures 5 and 6 summarize the seasonal UHI_{UCL} magnitudes for summer and winter based on the last classification. Figures are organized to give emphasis on the nocturnal UHI. Sunset and sunrise are considered to happen at 20:00 and 6:30 during summer, and 18:00 and 06:00 during winter. The UHI magnitude is determined by the maximum difference of the air temperature at each area (LCZ_X) against the results from the reference station (INMET – LCZ_9), as described in the section 2.4. Considering both seasons, an average difference of around 1°C is observed between summer and winter.

Figure 5 - Summer $UHI_{UCL,\ max}$ diurnal variation among LCZs.

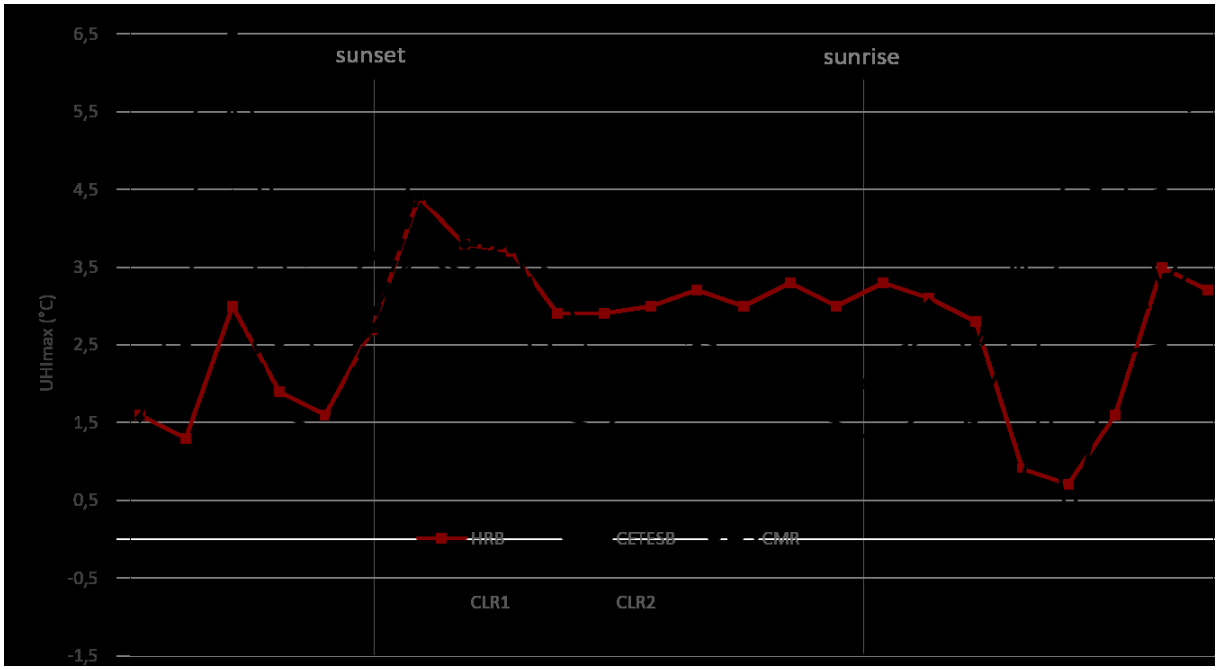

Source: Elaborated by the authors (2020)

Figure 6 - Winter $UHI_{UCL,\ max}$ diurnal variation among LCZs.

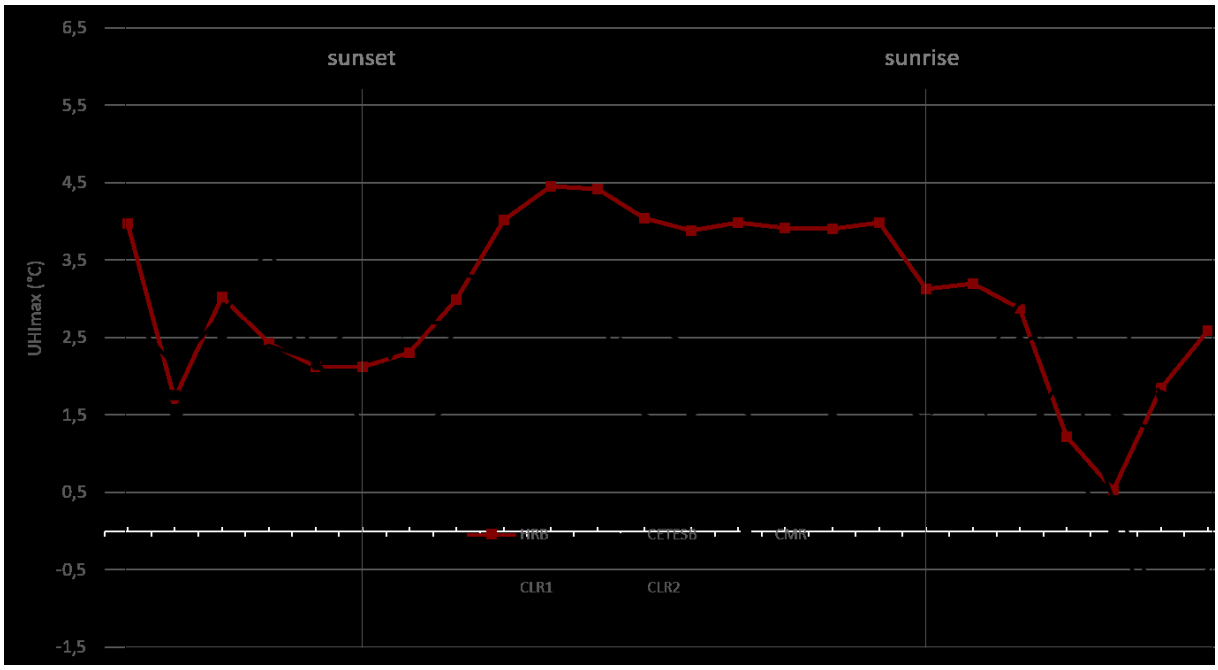

Source: Elaborated by the authors (2020)

To assist the discussion of the intra-urban UHI differences, wind flow taken at INMET and CETESB stations were summarized in Fig. 7 and 8 for summer and winter, respectively. In general, INMET showed a greater variance of direction and higher speed in both seasons compared with CETESB. During the dawn (00:00 – 05:00), the main wind directions come from

the southwest (SW) and west (W) for both seasons, while the northwest (NW) is common only in summer. For summer, the mean wind speed (m/s) was higher than winter, varying between 0,5 to 3,6. In the morning (06:00 – 11:00), the most frequent wind directions are west (W), southwest (SW), south (S), and southeast (SSE). At the afternoon (12:00 - 17:00), the sea breeze that comes from the southeast (SSE) is prevalent with wind speeds varying between 2.1 to 4.0. At night (18:00 - 23:00), while during the summer the main direction is from the east (E), for winter it comes from the west (W) and east (E). For both seasons, the eastward winds are greater than 2.1, while in other directions, the mean speed is ≤2.1. In contrast, CETESB is dominated mainly by two breeze patterns at mesoscale. The sea breeze blowing toward the mainland begins in the late morning and remains acting until the middle of the night when the land breeze starts to dominate until the early morning. Wind speed for both breezes varies from 0.5 – 2.6 m/s. While the sea breeze comes from south and southeast (S - SSE), the land breeze comes from northwest (NW) direction.

Figure 7 - Summer. Hourly wind flow from INMET (up) and CETESB (down).

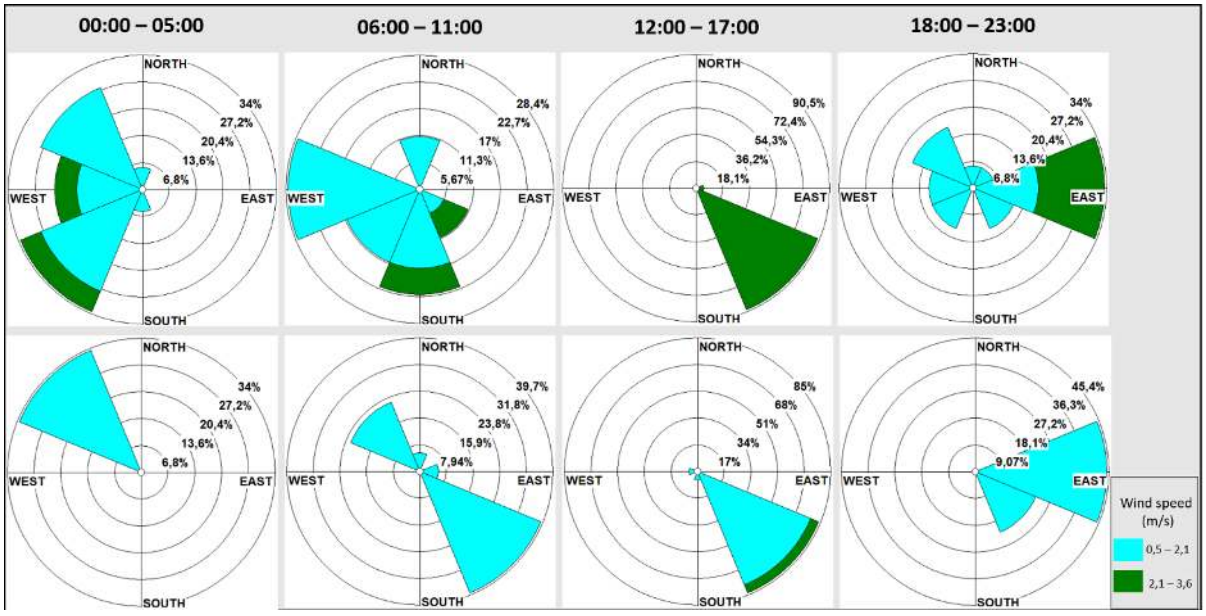

Source: Elaborated by the authors (2020)

Figure 8 - Winter. Hourly wind flow from INMET (up) and CETESB (down).

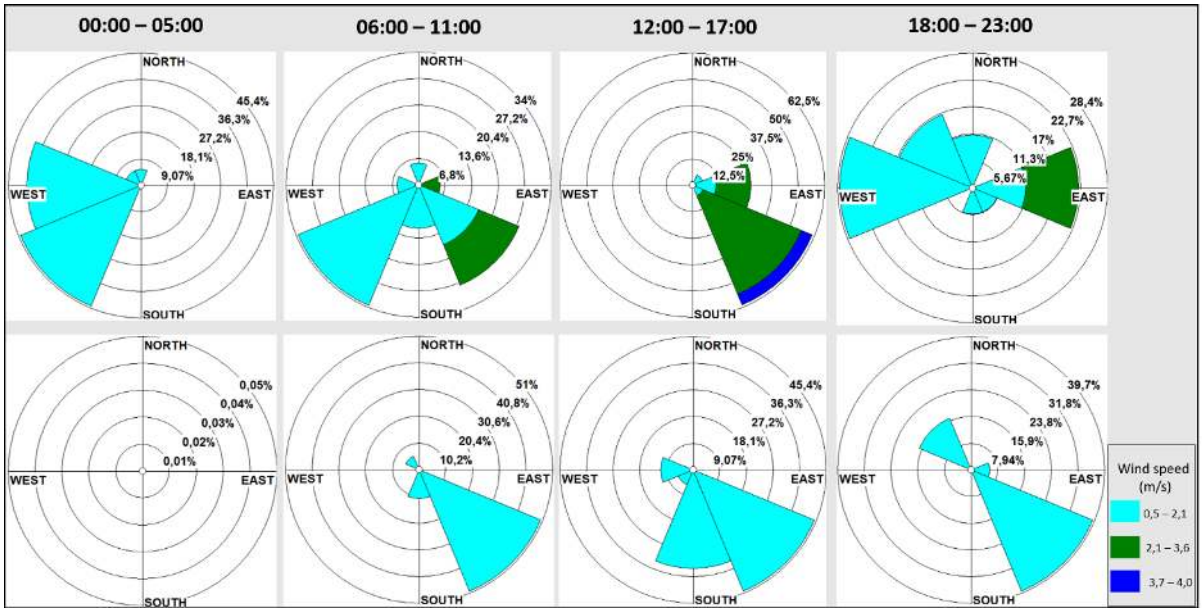

Source: Elaborated by the authors (2020)

DISCUSSION

To explain the seasonal variability of the observed nocturnal UHI values, i.e. ~1°C (summer < winter), it is essential to consider (1) the thermal admittance and (2) the weather. Higher soil moisture, higher heat storage capacity and thermal admittance make the rural surroundings thermally more homogenous than urban surfaces (OKE *et al*., 2017), which may explain the lower UHIs magnitude found here and in many tropical cities (Singapore, Colombo, Hong Kong, Kuala Lumpur, and Johor Bahru). Since summer represented the wettest period, i.e., 632,2mm (compared to 144,4mm in winter), those results may be related to moisture on the soil in the reference area (LCZ_9). Soils located in areas with more trees and grass are expected to present larger thermal admittance. Thus, the weaker warming/cooling rates tend to reduce the magnitude of the UHI (OKE *et al*., 2017). Those results agree with other studies at tropical cities, where the highest UHI magnitudes were found during the drier season, e.g., for Singapore, the maximum UHI is observed during June and the minimum during the wet period in January (CHOW & ROTH, 2006). In Seoul, Korea, the maximum magnitude of the heat island happened during autumn and winter, while during the humid summer it takes its minimum (KIM & BAIK, 2005).

Although other several weather elements are related to UHI, the main ones are wind and cloud (OKE *et al*., 2017). Through atmospheric transport and mixing, the wind is the main

driver of advection and turbulent exchange that limit horizontal and vertical temperature differences (OKE *et al*., 2017). Thus, the wind influences the UHI by altering the different cooling rates between urban and rural landscapes. This movement of air between these environments can result in a weakening of the urban-rural air temperature difference (MORRIS, SIMMONDS, and PLUMMER,2001). Cloud cover is an important modulating control of the UHI_{UCL}, since it affects the shortwave and longwave radiation, the main drivers of heating and cooling rates, respectively (MORRIS, SIMMONDS, and PLUMMER, 2001; OKE *et al*., 2017). At night, cloud cover provides natural insolation that absorbs and reemits infrared radiation downward, which is available for absorption by the surface and partially offsets the surface radiative loss. Through this process, the nocturnal radiative cooling may be slowed, hence decreases the differences in the observed temperatures between urban and non-urban areas (MORRIS, SIMMONDS, and PLUMMER, 2001). In this context, the seasonal UHI difference between the warm and cool season could be also explained due to thermal admittance and static stability, i.e., clearly, calm, and clear sky conditions, especially taking to account the UHI development in HRB (see Fig. 6).

Moreover, UHI exhibited a strong relationship between canyon geometry (e.g., H/W and SVF), often perceived in temperate cities (OKE, 1982). A comparison of nocturnal UHIs and urban geometry showed that UHI intensity increases with increasing height to width (H/W) ratios of street canyons (see e.g., OKE, 1982). Canyons with higher H/W generally absorb and store a significant amount of incoming shortwave radiation and lose less longwave radiation at night. SVF is related to the amount of visible sky at a given point, i.e. the sky available for a thermal energy dispersion. Clear relationship of it can be observed in the present study, as the location with the lowest value of SVF (HRB - 0.133) is associated with the highest nocturnal (specially at late night) value for both seasons during the nighttime.

The seasonal intra-urban differences during the daytime may be explained by solar exposure, shading, and vegetation. During the summer, higher solar radiation (~900W/m2) increases urban heat storage and consequently, the air temperature. As shown in Fig. 5, CLR2 promotes the highest UHI_{UCL} magnitudes (~6°C). This can be explained by both the heights of buildings and the devoid of vegetation. Low buildings receive much more shortwave radiation, which warms up the air at spaces between buildings more than in other LCZs. This result is illustrated by comparing SVF and the percentage of shading among LCZs (see Table 2). For example, at 17h, CLR2 that has the highest SVF (0.691) and the lowest percentage of shadow

(27) showed the highest UHI magnitude (6,5°). In the other hand, HRB, which represents the lowest SVF and the highest percentage of shadow (47), exhibited the lowest UHI (3°C) at the same time. The reason is that less solar radiation is absorbed at street level for lowest SVF, which provides shading during the daytime. Related to vegetation, most studies argue that the lack of greenery in the city tends to result in higher daytime air temperatures. The presence of vegetation in urban areas tends to reduce the maximum temperatures during the day, reducing the radiative changes at surface level. The effect of vegetation on urban warming phenomena not only manifests itself indirectly in the form of a reduction in the sensible heat flux from colder surfaces but also directly through evaporative cooling.

The existence of cool islands in cities has been already reported in numerous urban climatological studies. Lower urban temperatures may occur because of the less positive thermal balance in the specific urban zones than that of the reference station. For the present study, a persistent shadow occurs at the CETESB station (and CMR), which is probably the reason for the decrease in temperature in winter (Fig. 6). This may be observed in Fig. 9, which illustrates the hourly/monthly radiation from 2011 to 2019 based on CETESB data. This persistent shading in August (at 9h) and September (at 10h) result in a drop in the radiation, and consequently, in the air temperature. Since this could erroneously point toward the existence of a cool island (and related to the largest amount of vegetation, for example), the present study aims to reinforce that sometimes a more comprehensive evaluation of the meteorological conditions at both urban and reference stations should be done to guarantee the consistence of the analysis.

Figure 9 - CETESB monthly mean radiation (2011 – 2019).

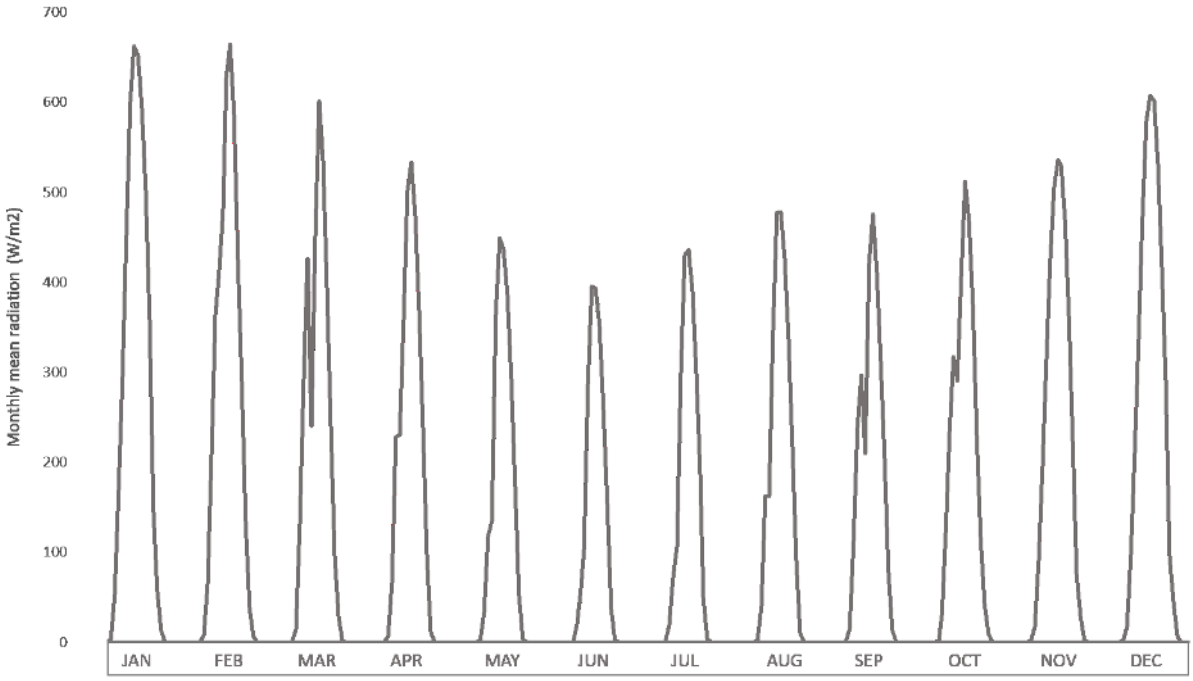

Source: Elaborated by the authors (2020)

Moreover, due to the sea breeze, the cool island has been reported in coastal cities, like in Bilbao (ACERO *et al*., 2012), Singapore (CHOW & ROTH), Sri Lanka (EMMANUEL & JOHANSSON, 2006), and Tel Aviv (MOUSAVI-BAYGI *et al*., 2010). However, as presented by Prata (2005) and how was observed in CETESB's air quality report (2014), the buildings on the edge of Santos form a barrier that hinders the penetration of the sea breeze. Prata (2005), at the time when the largest buildings had 26 floors, observed through measurements *in loco* that, at the seafront, the wind velocities were higher than those in different points behind the building's barrier. The CETESB report shows that its station located in a region with reduced roughness and closer to the coast ("Ponta da Praia") has a greater variation in wind direction and sea breeze intensity compared to the station further into the urban area (the station used in this study). It is noteworthy that nowadays, the buildings beside the coast have more than 30 floors, with heights up to 120 m. A similar result was exhibited when comparing wind flow from INMET and CETESB (Fig 7 and 8), as discussed previously.

CONCLUSION

As discussed, the different urban environments considered in the definition of LCZs show two distinct thermal responses that must be rethought to understand the role of

buildings in the city's climate strategy, especially in tropical coastal areas. Firstly, HRB enhances the mutual shading of buildings, which is beneficial during the daytime and can be contributed to the thermal comfort of dwellers. On the other hand, it can cause negative impacts, such as the highest nocturnal UHI and the obstruction of the penetration of the sea breeze to the other areas of the city. Secondly, since CLR is a common building pattern in tropical cities, this kind of construction contributes to the dispersion of thermal energy and longwave radiation during the night, they imply in higher temperatures during the day due to the absence of shading devices. This is further intensified by the lack of green areas, such as parks, or even trees on the sidewalks. On this way, the main findings from this study are:

(1) There is distinct seasonal variability in the UHI for all sites. Generally, higher UHI_{UCL} magnitudes were observed during the drier season (winter) and lower intensities during the wet season (summer). These results may be explained by the variability of moisture content at the reference station in summer and the static stability weather during the winter.

(2) Since HRB present the highest UHI at night for all seasons, the relationship between urban canyon geometry and UHI intensity is stronger.

(3) Shading and urban landscape features such as street trees could help to reduce the assimilated radiation and consequently the temperature. In this respect, the lack of shading devices and trees make CLR2 hotter than other LCZs during morning and afternoon.

(4) Radiation analyses should be more explored in studies related to UHI in coastal cities, since those regions represent areas with cloudiness varying throughout the day.

REFERENCES

AMORIM, M. C. C. T. Características do Clima Urbano de Presidente Prudente/SP. *In*: João Lima Sant'Anna Neto. (org.). **Os climas das cidades brasileiras**. Presidente Prudente: UNESP/FCT/Programa de Pós-graduação em Geografia, 2002. p. 165-196.

ASSIS, E. S; FROTA, A. B. Urban bioclimatic design strategies for a tropical city. **Atmospheric Environment**, Great Britain, v. 33, n.24, p. 4135-4142. 1999.

BENJAMIN, B *et al.* Mapping Local Climate Zones for a Worldwide Database of the Form and Function of Cities. ISPRS **Int. J. Geo-Inf**. p.199-219. 2015, DOI: 10.3390/ijgi4010199.

BENJAMIN, B *et al.* Generating WUDAPT level 0 data - current status of production and evaluation. **Urban Climate**, v.27,p. 24–45. DOI:https://doi.org/10.1016/j.uclim.2018.10.001. 2019.

BEJARAN, R. A; CAMILLONI I. A. Objective method for classifying air masses: an application to the analysis of Buenos Aires' (Argentina) urban heat island intensity'. **Theoretical and Applied Climatology**, v.74, p. 93–103. 2003.

BRAZILIAN INSTITUTE OF GEOGRAPHY AND STATISTICS (IBGE). **Cidades:** Santos-SP. Disponível em: http://cod.ibge.gov.br/3ZR. Acesso em: 10 Agosto de 2018.

CAMMILONI, I; BARRUNCAND, M. Temporal variability of the Buenos Aires, Argentina, urban heat island. **Theor Appl Climatol,** v.107, p.47–58. 2012.

CHOW, W; ROTH, M. Temporal dynamics of the urban heat island of Singapore. **International Journal of Climatology.** v. 26: 2243–2260. DOI: 10.1002/joc.1364. 2006.

CRAWFORD, B; KRAYENHOFF, E. S; CORDY, P. The urban energy balance of a lightweight low-rise neighborhood in Andallo, Chile. **Ther. Appl. Climatol** v.131, p.55-68. 2018.

DUARTE, D. Variáveis urbanísticas e microclimas urbanos - modelo empírico e proposta de um indicador. **Fórum Patrimônio**: Ambiente Construído e Patrimônio Sustentável (UFMG. Online), v. 3, p. 1-36, 2010.

DUARTE, D. Vegetation and climate-sensitive public places. *In*: Rohinton Emmanuel. (org.). **Urban climate challenges in the Tropics**: rethinking planning and design opportunities. 1ed.London: Imperial College Press, p. 111-162. 2016.

EMMANUEL R. Assessment of impact of land cover changes on urban bioclimate: the case of Colombo, Sri Lanka. **Architectural Science Review.** v.46, p.151–158. 2003.

EMMANUEL R. An Urban **Approach to Climate-Sensitive Design**: Strategies for the Tropics. Spoon Press: London. 2005a.

EMMANUEL R. Thermal comfort implications of urbanisation in a warm-humid city: the Colombo Metropolitan Region (CMR), Sri Lanka**. Building and Environment.** v.40, p.1591–1601. 2005b.

EMMANUEL, R; JOHANSSON, E. Influence of urban morphology and sea breeze on hot humid microclimate: the case of Colombo, Sri Lanka. **Climate Research**. v.30, p.189–200. 2006.

FENNER, D. *et al*. A. Spatial and temporal air temperature variability in Berlin, Germany, during the years 2001–2010. **Urban Climate**. v.10 (Part 2), p.308–331. 2014

FERREIRA, L. S; DUARTE, D. H. S. Exploring the relationship between urban form, land surface temperature and vegetation indices in a subtropical megacity. **Urban Climate**. v. 27, p. 105-123. 2019.

GEORGESON, L et al. Adaptation responses to climate change differ between global megacities. **Nature Climate Change**. v. 6, n. 6, p. 584-588. 2016.

KAWASHIMA, R. S *et al*. Análise das mudanças temporais de cobertura da terra na região portuária da Baixada Santista-SP e a proposição de modelos de dinâmica espacial. *In*: Simpósio Brasileiro de Sensoriamento Remoto (SBSR), 17., 2015, João Pessoa. **Anais**... São José dos Campos: INPE, 2015. Artigos, p. 1082-1089. DVD, On-line. ISBN 978-85-17-00076-8. Available in <http://www.dsr.inpe.br/sbsr2015/files/p0199.pdf>.

KIM, Y; BAIK, J. J. Spatial and temporal structure of the urban heat island in Seoul. **J. Appl. Meteorol**. v 44. 2005.

KOTHARKAR, R; BAGADE, A. Evaluating urban heat island in the critical local climate zones of an Indian city. **Landscape and Urban Planning**. v .169, p.92–104. 2018.

LOMBARDO, M. A. **Ilha de Calor na Metrópole Paulistana**. 1984. Tese (Doutorado em Geografia). Universidade de São Paulo, São Paulo. 1984.

MATZARAKIS, A. RAYMAN 1.2. Available in: freiburg.de/rayman/intro.htm 2009.

MATZARAKIS, A; RUTZ, F; MAYER, H. Modelling radiation fluxes in simple and complex environments: Basics of the RayMan model. **International Journal of Biometeorology**, v. 54, n. 2, p. 131–139. 2010.

MONTEIRO C. A de F. **Teoria e clima urbano**. 1976. Tese (Doutorado em Geografia). Universidade de São Paulo. Faculdade de Filosofia, Letras e Ciências Humanas, São Paulo. 1976. 181p.

MORRIS, K. I *et al*. Computational study of urban heat island of Putrajaya, Malaysia. **Sustainable Cities and Society**, v.19, p. 359–372. 2015.

MORRIS, C. J. G; SIMMONDS, I; PLUMMER, N. Quantification of the Influences of Wind and Cloud on the Nocturnal Urban Heat Island of a Large City. **Journal of Applied Meteorology**, v. 40(2), p.169-182. DOI: http://dx.doi.org/10.1175/15200450(2001)040%3C0169:QOTIOW%3E2.0.CO;2

MOUSAVI-BAYGI, M *et al*. The investigation of Tehran's heat island by using the surface ozone and temperature data. **Int. J. Appl. Environ. Sci**. v.5, p.189–200. 2010.

NICOL, J. E. High-resolution surface temperature patterns related to urban morphology in a tropical city: a satellite-based study. **Journal of Applied Meteorology**, v.35, p. 135–146. 1996.

NICOL, J. E; WONG, M. S. Modeling urban environmental quality in a tropical city. **Landscape and Urban Planning**, v.73. p. 49–58. 2005.

OKE, T. R *et al*. A. **Urban Climate**. Cambridge. 525p. 2017.

OKE, T. R. The energetic basis of the urban heat island. Q. J. R. **Meteorol. Soc**. v.108, p.1–24. 1982. DOI: https://doi.org/10.1002/qj.49710845502.

PALME, M; LOBATO, A; CLAUDIO, C. Quantitative Analysis of Factors Contributing to Urban Heat Island Effect in Cities of Latin-American Pacific Coast. *In*: **4th International Conference on Countermeasures to Urban Heat Island (UHI)**.2016. Procedia Engineering. p.99 – 206. 2016.

PERERA, N. G. R; EMMANUEL, R. A. “Local Climate Zone” based approach to urban planning in Colombo, Sri Lanka. **Urban Climate**. DOI:http://dx.doi.org/10.1016/j.uclim.2016.11.006.2016.

PRATA, A. R. **Impacto da altura de edifícios nas condições de ventilação natural do meio urbano**. 2005. Tese (Doutorado em Arquitetura e Urbanismo). Faculdade de Arquitetura e urbanismo. Universidade de São Paulo, São Paulo. 2005. DOI: 10.11606/T.16.2005.tde-20012010-113103.

RATTI C. F; RICHENS, P. Urban texture analysis with image processing techniques. *In*: **Proceedings of the CAADFutures99**, Atalanta, GA. 1999.

RIBEIRO, H. Heat island in Sao Paolo, Brazil: effects on health. **Critical Public Health**, v.15, p.147–156. 2005.

ROTH, M; CHOW, W. T. A historical review and assessment of urban heat island research in Singapore. **Singapore Journal of Tropical Geography**, v.33(3), p.381–397. 2012.

SAILOR, D. J; DIETSCH, N. The urban heat island mitigation impact-screening tool (MIST). **Environmental Modelling & Software**, v.22(10), p.1529–1541. 2007.

SECRETARY FOR PLANNING AND SUSTAINABLE DEVELOPMENT. **Caracterização Socioeconômica de São Paulo Região Metropolitana da Baixada Santista**, 2011. Governo do Estado de São Paulo. Available in:http://www.planejamento.sp.gov.br/noti_anexo/files/uam/trabalhos/RMBS.pdf. Acesso em: 10 de Agosto de 2018.

SHARMA, R *et al*. Application of Urban Climate for an Asian tropical city—The case of Delhi. *In*: **Living planet symposium**, v.740, p.210. 2016.

SIU, L. W; KART, M. A. Quantifying urban heat island intensity in Hong Kong SAR, China. **Environmental Monitoring and Assessment**, v.185(5), p.4383–4398. 2013.

SOUZA, L. C. L. Thermal environment as a parameter for urban planning. **Energy Sustainable Development**, v. XI, n.4, p. 44-53. 2007.

STEWARD, I. D; OKE, T. R. Local climate zones for urban temperature studies. **Bull. Am. Meteorol. Soc.**, v.93, p.1879-1900. 2012, DOI:10.1175/bams-d-11-00019.1.

STEWART, I. Global Cities Institute, University of Toronto, Toronto, Canada, LCZ metric. Personal communication, 2016.

STEWART, I.D; OKE, T.R; KRAYENHOFF, E.S. Evaluation of the “local climate zone” scheme using temperature observations and model simulations. **Int. J. Climatol**., v.34, p.1062–1080. 2014.

TAN, Z; LAU, K. K; NG, E. Urban tree design approaches for mitigating daytime urban heat island effects in a high-density urban environment. **Energy and Buildings**, v.114, p.265–274. 2016.

THOMAS, G *et al*. Analysis of urban heat island in Kochi, India, using a modified local climate zone classification. **Procedia Environmental Sciences**, v.21, p.3–13. 2014.

TSO, C. P. A survey of urban heat island studies in two tropical cities. **Atmospheric Environment**, v.30, p.507–519. 1996.

UNITED NATIONS. Desa/Population Division. **World population/urbanization prospects**. Available in: https://population.un.org/wup/Maps/. Acesso em 10 de Agosto de 2018.

WONG, N. H; TAN, Y. P; LOH, L. F. Historical analysis of long-term climatic data to study urban heat islands in Singapore. **Architectural Science Review**, v.48, p.25–40. 2005.

WONG, N.H; YU, C. Study of green areas and urban heat island in a tropical city. **Habitat International**, v.29, p.547–558. 2005.